Acta Oceanol. Sin., 2018, Vol. 37, No. 3, P. 51–62
DOI: 10.1007/s13131-017-1102-3
http://www.hyxb.org.cn
E-mail: hyxbe@263.net

On the subtropical Northeast Pacific mixed layer depth and its influence on the subduction

XIA Ruibin[1]*, LIU Chengyan[1], CHENG Chen[1]

[1] Polar Climate System and Global Change Laboratory, Nanjing University of Information Science & Technology, Nanjing 210044, China

Received 4 June 2017; accepted 29 July 2017

©The Chinese Society of Oceanography and Springer-Verlag Berlin Heidelberg 2018

Abstract

The present climate simulations of the mixed layer depth (MLD) and the subduction rate in the subtropical Northeast Pacific are investigated based on nine of the CMIP5 models. Compared with the observation data, spatial patterns of the MLD and the subduction rate are well simulated in these models. The spatial pattern of the MLD is nonuniform, with a local maximum MLD (>140 m) region centered at (28°N, 135°W) in late winter. The nonuniform MLD pattern causes a strong MLD front on the south of the MLD maximum region, controls the lateral induction rate pattern, and then decides the nonuniform distribution of the subduction rate. Due to the inter-regional difference of the MLD, we divide this area into two regions. The relatively uniform Ekman pumping has little effect on the nonuniform subduction spatial pattern, though it is nearly equal to the lateral induction in values. In the south region, the northward warm Ekman advection (-1.75×10^{-7} K/s) controls the ocean horizontal temperature advection (-0.85×10^{-7} K/s), and prevents the deepening of the MLD. In the ensemble mean, the contribution of the ocean advection to the MLD is about –29.0 m/month, offsetting the sea surface net heat flux contribution (33.9 m/month). While in the north region, the southward cold advection deepens the MLD (21.4 m/month) as similar as the heat flux (30.4 m/month). In conclusion, the nonuniform MLD pattern is dominated by the nonuniform ocean horizontal temperature advection. This new finding indicates that the upper ocean current play an important role in the variability of the winter MLD and the subduction rate.

Key words: mixed layer depth, mixed layer depth front, subduction, horizontal temperature advection, nonuniform

Citation: Xia Ruibin, Liu Chengyan, Cheng Chen. 2018. On the subtropical Northeast Pacific mixed layer depth and its influence on the subduction. Acta Oceanologica Sinica, 37(3): 51–62, doi: 10.1007/s13131-017-1102-3

1 Introduction

The ocean mixed layer is a striking and nearly universal feature of the open ocean, with nearly vertically uniform salinity, temperature and density. The mixed layer links the atmosphere to the deep ocean and plays a critical role in climate variability. Atmospheric fluxes of momentum, heat and freshwater through the ocean surface drive vertical mixing and provide the source of almost all oceanic motions (de Boyer Montégut et al., 2004; Dong et al., 2008). The ocean mixed layer is often defined as the layer where the temperature, density or their vertical gradients smaller than some values near the sea surface. So ocean mixed layer depth (MLD) is one of the most important quantities of the upper ocean as it defines the quasi-homogeneous surface region of density that directly interacts with the atmosphere (Kara et al., 2003).

So far, there are many researches about the variability and dynamics of the MLD with different time scales in different oceans (Levitus, 1982; Monterey and Levitus, 1997; Carton and Giese, 2008). The temporal variability of the MLD is usually linked to many processes occurring in the mixed layer (surface forcing, lateral advection, etc.). For example, seasonal variability of the MLD in the Kuroshio Extension is controlled by sea surface heat flux (Qiu and Kelly, 1993). According to the mixed layer temperature equation, the sea surface heat flux, vertical pumping and ocean advection all impact on the mixed layer temperature seasonal variability in the three North Pacific subtropical mode water formation regions, but the contribution of ocean advection is relatively small (Pan et al., 2011). While the mixed layer temperature seasonal variability is not absolutely consistent with the MLD variability, so it is necessary to explore the contributions of the three factors to the MLD seasonal variability. The annual and decadal variabilities of the MLD in the North Pacific is also connect with the variabilities of wind and heat flux induced by the Pacific Decadal Oscillation (Deser and Blackmon, 1995; Qiu and Chen, 2006; Dawe and Thompson, 2007).

Until now, a few previous studies focus on the effect of the ocean advection. Xie at al. (2010) pointed out that the ocean advection influences the SST change after global warming. The intensification of the South Pacific subantarctic mode water (SAMW) is mainly caused by a deepening of the MLD and a strengthening of the advection in warm climate (Liu and Wu, 2012; Liu and Wang, 2014). Coincidentally, using a model simulation result, it is proved that the ocean horizontal temperature advection plays a critical role in the response of the MLD to global

Foundation item: The National Natural Science Foundation of China under contract Nos 41606217, 41675064 and 41406214; the Scientific Research Foundation for the Talent Start-Up of University of Information Science and Technology under contract No. 2015r043; the Open Fund of the Key Laboratory of Research on Marine Hazards Forecasting under contract No. LOMF1702; the China Scholarship Council under contract No. 201708320046.
*Corresponding author, E-mail: xiarb@nuist.edu.cn

warming at the eastern subtropical Pacific mode water (ESTMW) formation region (Xia et al., 2015). These researches remind us that the ocean advection may be important for the MLD variability in some oceans.

Ocean ventilation, including subduction and obduction process, is a key component of global oceanic circulation. Subduction and obduction have been widely used as tools describing kinematical and dynamical processes coupling the mixed layer and the ocean interior. The spatial pattern and temporal variation of the MLD both play important roles in the subduction and obduction process (Stommel, 1979; Woods, 1985; Marshall et al., 1993). So that many products by the subduction process are indirectly dominated by the MLD, such as the mode water. While the effective subduction generally occurs in late winter or early spring, when the MLD reaches its local maximum (Marshall et al., 1993), we use the February-March mean to analyze the subduction mechanism in this paper.

There are many studies about the subduction rate and mode water formation mechanism. The MLD plays an important role in the lateral induction, then influences the subduction rate. Generally, sea surface net heat flux or surface wind field are considered as key factors on the MLD, and impact on the formation of the subduction rate and mode water (Qu and Chen, 2009; Hu et al., 2011; Xu et al., 2012). For example, both subantarctic mode water (SAMW) and Antarctic Intermediate Water (AAIW) are increased under intensified westerlies and increased heat loss, and the lateral induction term change plays a dominant role due to the deepening of the MLD (Liu et al., 2017). While the ocean advection may play an important role in the MLD change as mentioned above, how does the ocean advection contribute to the subduction? In addition, these researches point out the importance of the MLD front on the connection between MLD and subduction. But how does the MLD change influence the MLD front? These questions are not known clearly.

There are two MLD local maximum regions in subtropical North Pacific. The previous studies usually care more about the western region with relatively deeper MLD (Xu et al., 2012). While the eastern MLD local maximum region, accompanying by the subduction local maximum and formation of the ESTMW, is also important. Only a few researches focused on the eastern region and pointed out the possible significance of the MLD front on the subduction (Xie et al., 2000; Suga et al., 2004). Xia et al. (2015) also showed the importance of the MLD front and horizontal temperature advection change on the response of the subduction and ESTMW to global warming, but that result was just based on one single model. In this paper, we use nine of the Coupled Model Intercomparison Project Phase 5 (CMIP5) models to exhibit the MLD spatial pattern in detail. The first basic scientific question is: what are the characteristics and mechanisms of the MLD climatology in the subtropical Northeast Pacific? We find a special nonuniform spatial pattern of the MLD in the subtropical Northeast Pacific, which could induce a strong MLD front. Both the Ekman pumping and Ekman advection caused by the surface wind field make contributions to the MLD variability. Especially, the north-south Ekman advection influences the upper ocean horizontal temperature advection and dominates the nonuniform spatial pattern of the MLD. Connected with the subduction porcess, we will discuss the second scientific question: how does the MLD spatial distribution influence the subduction in the subtropical Northeast Pacific Ocean? We propose that, the spatial nonuniform distribution of the MLD forms the strong MLD front, which should play an important role in the subduction process by the lateral induction. So the region where MLD front exists would become the major source of the subduction and mode water. The present study investigates this assertion.

The rest of the paper is organized as follows. A brief description of data and primary methods is introduced in Section 2. We examine the MLD characteristics in the CMIP5 models compared with the observation data in Section 3 and explore the mechanisms in Section 4. The influence of the MLD on the subduction process is investigated in Section 5. Finally, Section 6 presents the summary and conclusions.

2 Data and methods

2.1 *Data*

The present study primarily uses the output from nine global coupled climate models (Table 1) as part of the CMIP5 (Dunne et al., 2012; Taylor et al., 2012). We choose the historical simulation to reflect the twentieth-century climate forced by observed atmospheric composition changes (Taylor et al., 2012). The present-day climatology is taken from 1951 to 2000 averaged. The spatial resolution varies between models and within the same model for atmospheric and oceanic variables. To facilitate comparison with each model and observations, we interpolated them onto a 1°×1° latitude-longitude grid. We investigate both the common features (ensemble mean) and the inter-model difference among models, focusing on the MLD variability and dynamics. The same member run (R1i1p1) is chosen in all models. The model output is freely available from the Program for Climate Model Diagnosis and Intercomparison (PCMDI) at the Lawrence Livermore National Laboratory (http://cmip-pcmdi.llnl.gov/cmip5/).

To examine the model data, the monthly climatology Argo and NODC (Levitus) World Ocean Atlas 1994 data (Levitus and Boyer 1994) are also used. These data are both 1°×1° gridded and from the Asia-Pacific Data Research Center (APDRC, http://apdrc.soest.hawaii.edu/).

2.2 *Methods*

The temperature of the mixed layer and MLD variabilities is

Table 1. Nine models analyzed in this study from CMIP5

	Model	Institution	Country
a	CCSM4	National Center for Atmospheric Research	USA
b	CNRM-CM5	Centre National de Recherches Meteorologiques	Europe
c	GFDL-ESM2G	NOAA / Geophysical Fluid Dynamics Laboratory	USA
d	GFDL-ESM2M	NOAA / Geophysical Fluid Dynamics Laboratory	USA
e	IPSL-CM5A-LR	Institute Pierre-Simon Laplace	France
f	IPSL-CM5A-MR	Institute Pierre-Simon Laplace	France
g	MIROC-ESM	the University of Tokyo	Japan
h	MPI-ESM-LR	Max Planck Institute for Meteorology	Germany
i	MRI-CGCM3	Meteorological Research Institute	Japan

calculated as (Qiu and Kelly, 1993; Qiu, 2002):

$$\frac{\partial T_{\mathrm{m}}}{\partial t}=\frac{Q_{\mathrm{net}}}{\rho_0 c_{\mathrm{p}} h_{\mathrm{m}}}-\vec{u}_{\mathrm{m}}\cdot\nabla T_{\mathrm{m}}-\frac{\omega_{\mathrm{e}}\left(T_{\mathrm{m}}-T_{\mathrm{d}}\right)}{h_{\mathrm{m}}}, \tag{1}$$

$$\frac{\partial h_{\mathrm{m}}}{\partial t}+\vec{u}_{\mathrm{m}}\cdot\nabla h_{\mathrm{m}}=\mathrm{A}_{\mathrm{h}}\nabla^2 h_{\mathrm{m}}+\omega_{\mathrm{e}}, \tag{2}$$

$$Q_{\mathrm{net}}=Q_{\mathrm{lat}}+Q_{\mathrm{sen}}+Q_{\mathrm{s}}+Q_{\mathrm{l}}. \tag{3}$$

In Eq. (1), the four terms represent the temperature tendency, sea surface horizontal temperature flux forcing, ocean horizontal temperature advection and vertical entrainment separately. Similarly, the four terms in Eq. (2) represent the MLD tendency, MLD advection, horizontal diffusion and vertical entrainment respectively. T_{m} means the mixed layer average temperature, h_{m} is the MLD, c_{p} is the specific heat capacity of sea water, ρ_0 is the reference density, $\vec{u}_{\mathrm{m}}$ is the horizontal ocean velocity, ω_{e} is the vertical entrainment velocity, T_{d} is the temperature at the base of the MLD, and A_{h} is the horizontal diffusivity. The sea surface net heat flux Q_{net} is composed of the lateral heat flux Q_{lat}, sensible heat flux Q_{sen}, short-wave radiation Q_{s} and long-wave radiation Q_{l} (Kraus, 1972).

In this paper, we use Eqs (1) and (2) to infer the following equation:

$$\frac{\partial h_{\mathrm{m}}}{\partial t}=-\vec{u}_{\mathrm{m}}\cdot\nabla h_{\mathrm{m}}+A_{\mathrm{h}}\nabla^2 h_{\mathrm{m}}+\left(-\frac{\partial T_{\mathrm{m}}}{\partial t}+\frac{Q_{\mathrm{net}}}{\rho_0 c_{\mathrm{p}} h_{\mathrm{m}}}-\vec{u}_{\mathrm{m}}\cdot\nabla T_{\mathrm{m}}\right)\times\frac{h_{\mathrm{m}}}{\left(T_{\mathrm{m}}-T_{\mathrm{d}}\right)}. \tag{4}$$

Here we define two vaiables:

$$h'_{\mathrm{q}}=\frac{Q_{\mathrm{net}}}{\rho_0 c_{\mathrm{p}}\left(T_{\mathrm{m}}-T_{\mathrm{d}}\right)}, \tag{5}$$

$$h'_{\mathrm{t}}=\vec{u}_{\mathrm{m}}\cdot\nabla T_{\mathrm{m}}\times\frac{h_{\mathrm{m}}}{\left(T_{\mathrm{m}}-T_{\mathrm{d}}\right)}, \tag{6}$$

where h'_{q} and h'_{t} represent the contribution of the sea surface net heat flux and ocean horizontal temperature advection on the MLD change respectively, with unit m/month.

The subduction rate is defined as (Williams, 1991; Xie et al., 2011; Xu et al., 2012):

$$S_{\mathrm{mean}}=-\vec{u}_{\mathrm{m}}\cdot\nabla h_{\mathrm{m}}+w_{\mathrm{e}}, \tag{7}$$

where $-\vec{u}_{\mathrm{m}}\cdot\nabla h_{\mathrm{m}}$ is the lateral induction, and w_{e} is the Ekman pumping velocity. The Ekman pumping velocity can be defined as $w_{\mathrm{e}}=\mathrm{curl}_z\left(\tau/f\right)/\rho_0$ (Pond and Pickard, 1983), where τ is the wind stress, and f is the Coriolis parameter.

In addition, the ocean horizontal temperature advection (HTA) could be resolved into two terms (Qiu, 2002):

$$HTA=\vec{u}\cdot\nabla T=u\frac{\partial T}{\partial x}+v\frac{\partial T}{\partial y}=\vec{u}_{\mathrm{e}}\cdot\nabla T+\vec{u}_{\mathrm{g}}\cdot\nabla T, \tag{8}$$

where $\vec{u}_{\mathrm{e}}$ and $\vec{u}_{\mathrm{g}}$ are the Ekman velocity and geostrophic velocity. Here we use $HTA_{\mathrm{e}}=\vec{u}_{\mathrm{e}}\cdot\nabla T$ to represent for the Ekman advection, and $HTA_{\mathrm{g}}=\vec{u}_{\mathrm{g}}\cdot\nabla T$ for the geostrophic advection.

The MLD horizontal gradient is calculated as:

$$h_{\mathrm{grad}}=\nabla h_{\mathrm{m}}=\frac{\partial h_{\mathrm{m}}}{\partial x}\vec{i}+\frac{\partial h_{\mathrm{m}}}{\partial y}\vec{j}, \tag{9}$$

here the unit of h_{grad} is m/km.

3 The climatology characteristics of the subtropical Northeast Pacific MLD

This section examines the reproducibility of the subtropical Northeast Pacific MLD in CMIP5 models for present day climate. We first examine the MLD climatology from the nine CMIP5 models historical simulation during 1951–2000 compared with the observation data, then discuss the nonuniform spatial pattern of the MLD and its influence on the MLD front. Thirdly, the MLD seasonal variability is also examined. Finally we show the inter-model variability.

3.1 *The MLD climatology characteristics*

In this paper, the MLD is defined as the depth at which the water density is 0.1 kg/m^3 denser than the sea surface (Luo et al., 2009). We have examined the temperature and salinity profiles to confirm that the MLD definition is suitable in the subtropical Northeast Pacific. The simulated MLD from different models and that obtained from Argo and Levitus observation data are shown in Fig. 1. The modeling results are similar to those of previous modeling studies (Luo et al., 2009; Hu et al., 2011), and observation results are similar to those of previous observational studies (Toyoda et al., 2004; Suga et al., 2004). Compared with the Levitus (Fig. 1k) and Argo (Fig. 1l) data, all modeling results (Figs 1a–i) could simulate the MLD spatial pattern accurately and similarly. Thus the modeling ensemble mean result (Fig. 1j) is also similar to the observation result, and is used to analyze the MLD pattern as its representativeness. The MLD spatial pattern is nonnuiform, with a maximum (>140 m) appearing at (28°N, 135°W) in late winter. The MLD shoals slowly from the maximum region northward, but quickly southward to about 40–60 m. This phenomenon forms a narrow transition zone called the MLD front (Xie et al., 2000) on the south of the MLD maximum region (Fig. 1, black points). In another word, the MLD has a inter-regional difference, which is much deeper (>140 m) in the north region and relatively shallower (<60 m) in the south region. Thus we divide this area into two regions, taking the MLD front as the boundary. The two regions are called “north region” (23°–33°N, 145°–125°W, as the MLD maximum region) and “south region” (12°–23°N, 145°–120°W, as the shallower MLD region on the south of the MLD front) respectively. Dividing into two regions will be helpful to explore the mechanism of the MLD spatial pattern in Section 4. In a word, the spatial pattern of the MLD is nonuniform, causing a strong MLD front on the south of the MLD maximum region.

3.2 *The MLD front*

We investigated the position and intensity of the MLD front in this region. When the MLD reaches deepest, the front will reach the strongest. So the MLD front position is defined as the place where the MLD horizontal gradient reaches maximum in late winter (February–March), and the intensity is defined as the maximum gradient. The MLD horizontal gradient is calculated by Eq. (9) in Section 2. The MLD front positions are similar in all

the models and observation (Fig. 1, black points). The MLD front stretches banded near east-west direction, especially at (150°W to 120°W). The ensemble mean MLD front intensity maximum is about 0.19 m/km (Fig. 2b). The inter-model difference of the MLD front intensity is obvious, and the details will be discussed. We will demonstrate this distribution of the MLD front has significant influence on the winter subduction process in Section 4.

3.3 *The Seasonal cycle of the MLD*

According to our research, the inter-model variability of the

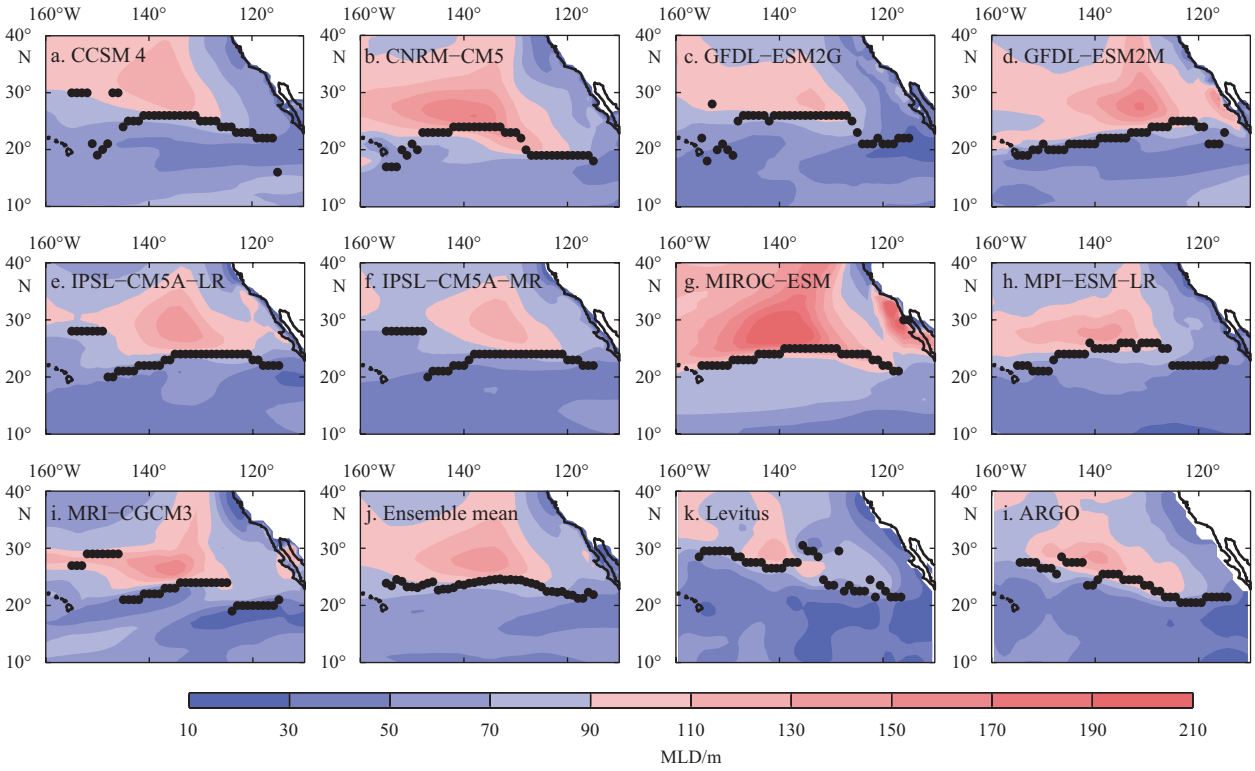

Fig. 1. The February-March mean MLD (shading, interval: 20 m) and the position of the MLD front (black points) from historical simulation of the nine models (a–i) and ensemble mean result (j), compared with two observation results (k, l).

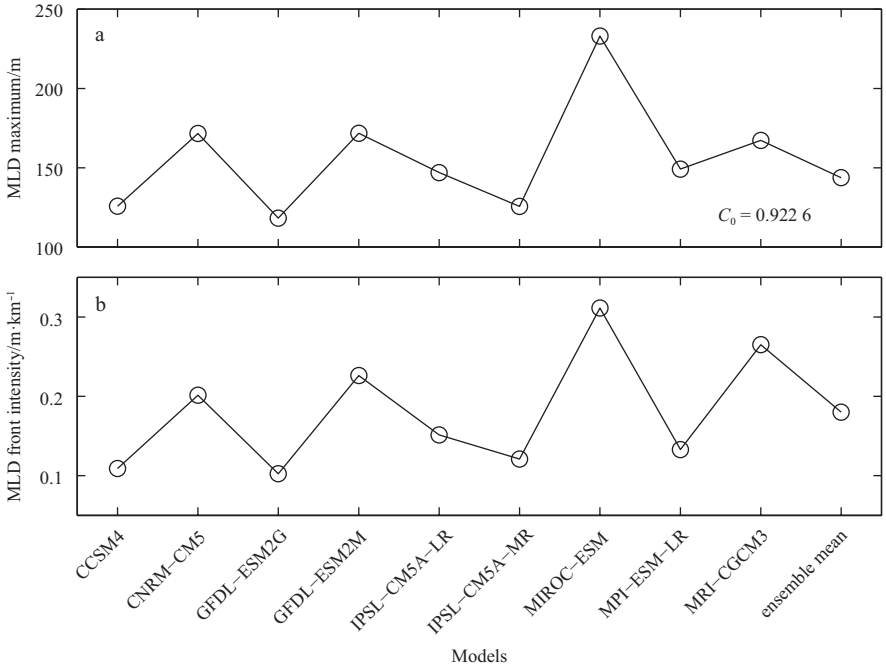

Fig. 2. The MLD maximum (a) and the intensity of the MLD front (b) mean during February–March in historical simulation of the nine models and ensemble mean result. C_0=0.922 6 means the correlation coefficient of the two plots.

MLD seasonal cycle is not large. So we choose the ensemble mean result to represent the seasonal cycle of the MLD (Fig. 3), which is comparable to the observation (not shown). The MLD deepens from October and reaches its maximum in February and March in the modeling results; subsequently, it starts to shoal until it reaches its minimum in summer and early autumn (July to September). This result is consitent with one single model simulation result (e.g., Xia et al., 2015) and the observation results (e.g., de Boyer Montégut et al., 2004). The rapid shoaling of the MLD makes it possible for the water to be subducted into the pycnocline by the advection and carried away by the subtropical gyre (Hu et al., 2011; Xia et al., 2015).

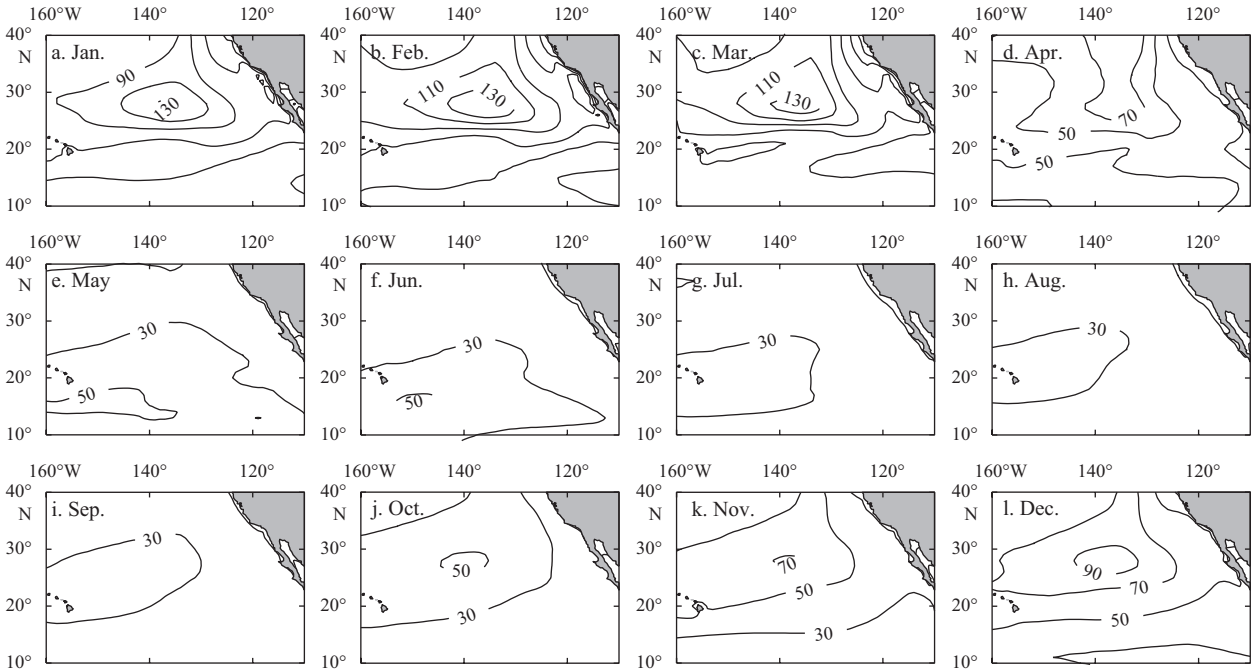

Fig. 3. The MLD (contours, interval: 20 m) seasonal variability in historical simulation of the CMIP5 ensemble mean.

3.4 *The Inter-model difference*

The inter-model difference of the MLD generally appears in the maximum values and their positions in east-west direction. The inter-model difference of MLD maximum is shown in Fig. 2a. For example, the MLD maximum is more than 240 m in the MIROC-ESM, but only about 110 m in the GFDL-ESM2G. In addition, the locations of the MLD maximum in CNRM-CM5, MIROC-ESM and MPI-ESM-LR are similar to that in the observation (28°N, 140°W), but at (28°N, 135°W) in GFDL-ESM2G and GFDL-ESM2M. As the MLD front positions are similar in all the models, the inter-model difference appears in the intensity (Fig. 2b). It is easy to find the high correlation between the inter-model difference of the MLD front intensity and the inter-model difference of the MLD maximum (Fig. 2a), and the correlation coefficient is over 0.92. For example, the maximum of the MLD (over 240 m) and MLD front intensity (over 0.30 m/km) appear in the same model (MIROC-ESM). In conclusion, the inter-model variability of the nonuniform MLD spatial pattern causes the difference of the MLD front intensity among models, providing further evidence for nonuniform MLD effect on MLD front.

4 Mechanisms of the nonuniform MLD spatial pattern

As Section 3 shows, the MLD spatial pattern is nonuniform in both modeling simulation and observation data, and this nonuniform pattern causes the formation of the strong banded MLD front on the south of the MLD maximum region. So how does this MLD nonuniform pattern occur in present climatology? The MLD spatial pattern is controlled by the upper ocean stratification. The deepening MLD is always consistent with the weakening stratification. While upper ocean stratification is decided by many factors, such as the surface wind field, sea surface net heat flux and horizontal temperature advection in the upper ocean. Because the salinity effect is relatively small in this region, the evaporation minus precipitation flux is not considered in this paper. In single CMIP5 model, such as GFDL-ESM2M, it has been proved that the banded changing ocean horizontal temperature advection would obviously influence the banded changing of the MLD, as a response to global warming (Xia et al., 2015). This section will explore the factors mentioned above and focus on the contribution of the ocean horizontal temperature advection quantitatively, using modeling results. We will discuss the common mechanisms with ensemble mean results firstly, and then show the inter-model difference.

4.1 *Ekman pumping*

As shown in Fig. 4a, the spatial pattern of the Ekman pumping caused by sea surface wind stress is generally similar to the spatial pattern of the winter MLD, which indicates that the Ekman pumping decides the general pattern of the winter MLD. The wind stress induces a downward Ekman pumping, and causes the MLD deepening. However, the Ekman pumping maximum occurs to the south of the MLD maximum region. The Ekman pumping is uniform in its maximum region (Fig. 4a, shading, $>1.5\times10^{-6}$ m/s), but the MLD shoals quickly from north to south in the same region. This interesting phenomenon indicates that the Ekman pumping is not the only mechanism on the MLD spatial pattern. In addition, the inter-model difference of the Ekman pumping is not so large actually (not shown), thus it

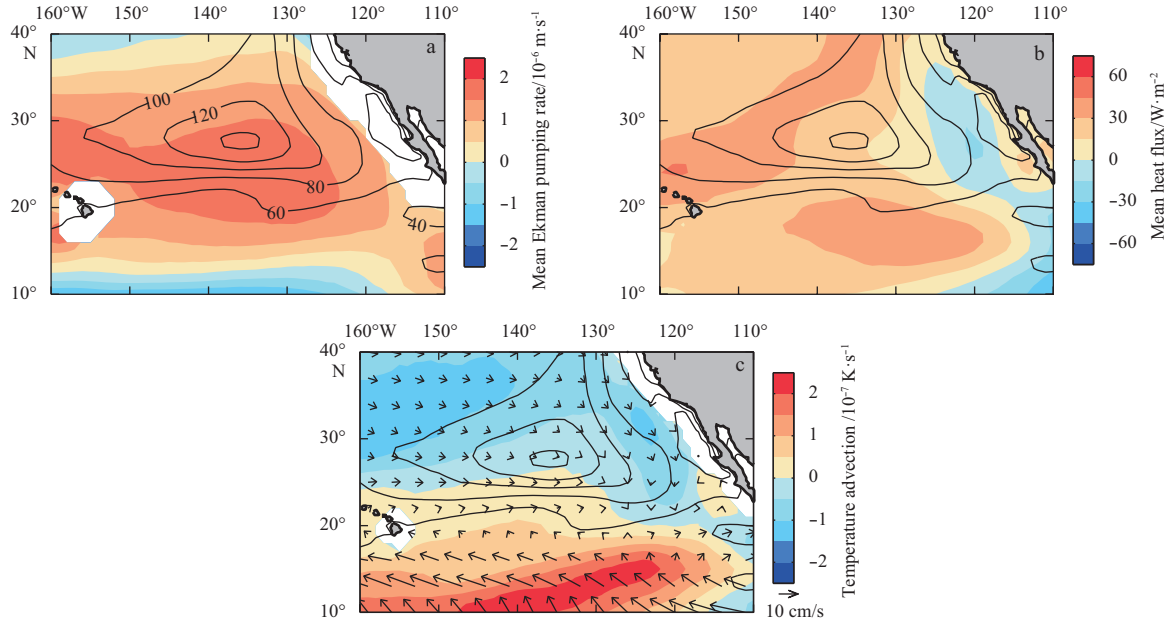

Fig. 4. Ensemble mean during February–March in historical simulation (1950–2000): a. Ekman pumping rate (shading in 10^{-6} m/s, downward is positive); b. net ocean-atmosphere heat flux (shading in W/m^2); and c. vertical average horizontal temperature advection (0–50 m average, shading in 10^{-7} K/s) and current (0–50 m average, arrows). The contours indicate MLD mean during February–March (contours, interval: 20 m).

would not be the main reason of the MLD inter-model difference.

4.2 *The sea surface net heat flux and ocean horizontal temperature advection*

As the Ekman pumping is not the only mechanism on the MLD spatial pattern, we discuss the contributions of the sea surface net heat flux and ocean horizontal temperature advection. In this paper, the positive values of the sea surface net heat flux mean that ocean losses heat, and are conductive to the deepening of the MLD. While the positive horizontal temperature advection in the upper ocean increases the vertical temperature difference, enhances the stratification, and finally shoals the MLD. Figures 4b and c show the contributions of the sea surface net heat flux and ocean horizontal temperature advection. As mentioned in Section 3, we analyze the contributions of the sea surface net heat flux and ocean horizontal temperature advection in the "north region" and "south region" separately. In the north region, both the net heat flux and cold advection are helpful to deepen the MLD, but not completely consistent with the MLD spatial pattern. Compared with the Ekman pumping, it indicates that all these three factors have positive contributions to the deepening of the MLD, and they decide the MLD spatial pattern in the north region together. In the south region, the significant warm advection plays a major role in limiting the deepening of the MLD (<60

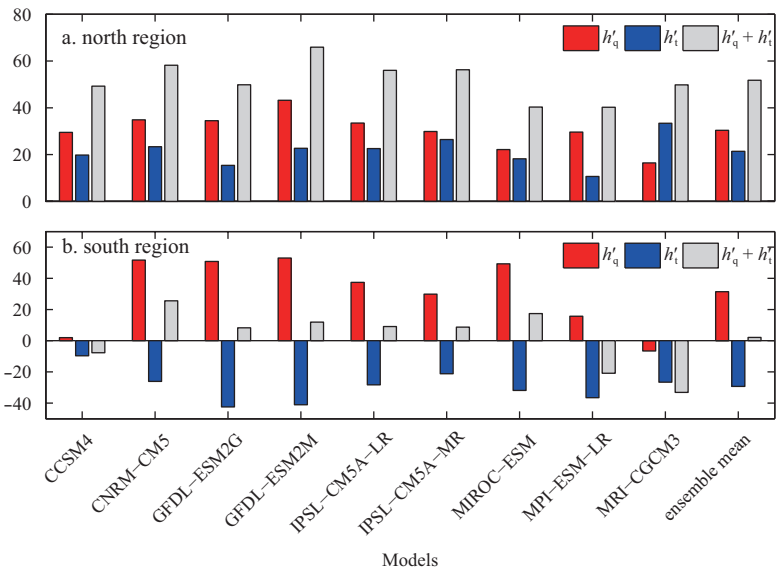

Fig. 5. The regional average h'_q (red bars), h'_t (blue bars) and $h'_q + h'_t$ (gray bars) (m/month) during February–March in historical simulation of the nine models and ensemble mean result.

m), though both downward Ekman pumping and positive net heat flux are useful to deepen the MLD. As the contribution of the net heat flux on increasing the MLD is larger in the south region than that in the north region, and the Ekman pumping equally contributes to the deepening of the MLD in the two regions, we indicate the inter-regional difference of the MLD is mainly due to the inter-regional difference of the horizontal temperature advection. As a result, the strong MLD front is induced and promotes the subduction in late winter greatly.

To compare the contribution of sea surface net heat flux and ocean horizontal temperature advection quantitatively, regional average $h_q^{'}$ and $h_t^{'}$ are calculated from Eqs (5) and (6), which rep-

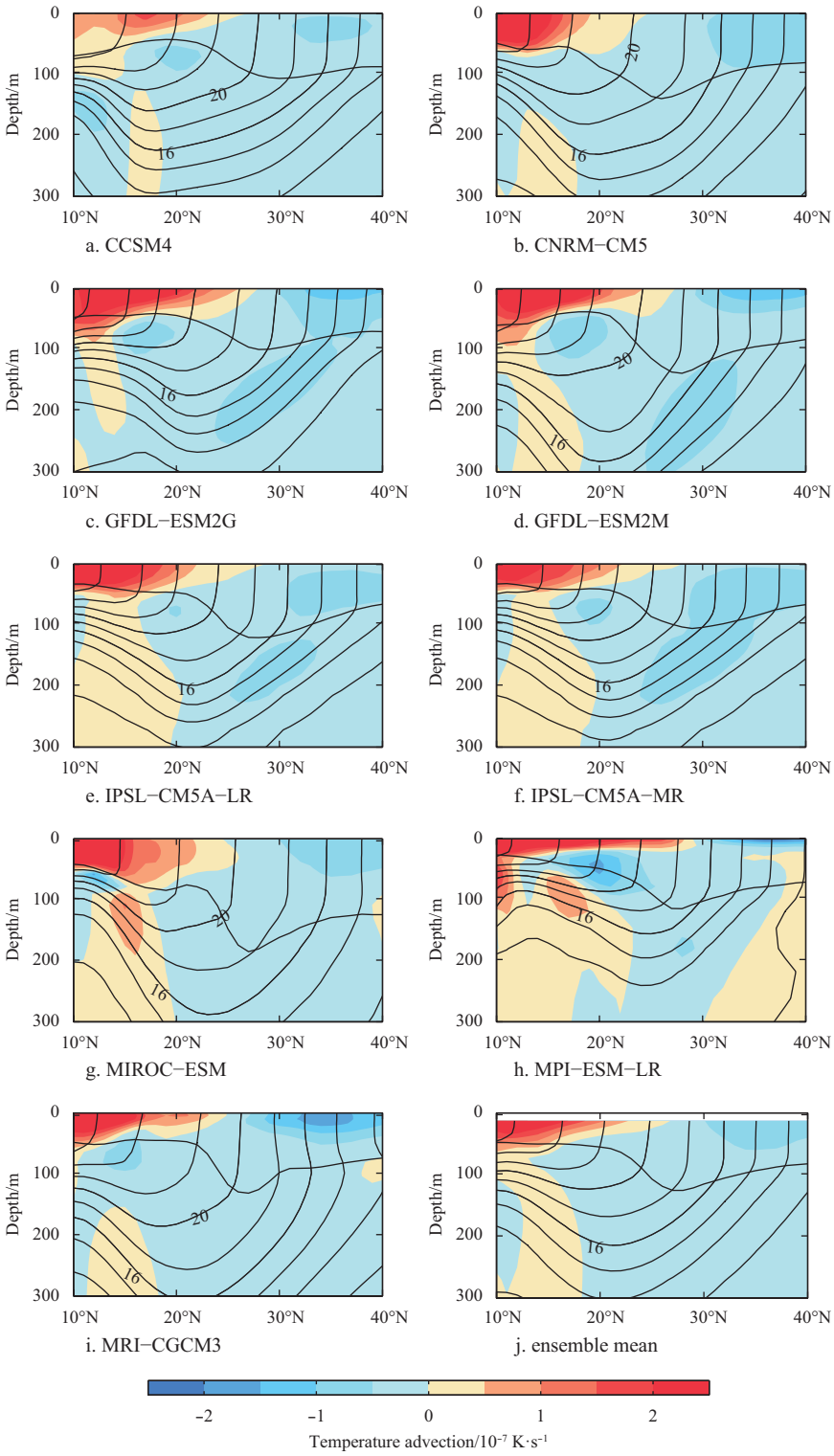

Fig. 6. Vertical-latitude section of the horizontal temperature advection (shading in K/s) and temperature (contours, interval: 2 K) along 145° to 125°W mean during February–March in historical simulation of the nine models (a–i) and ensemble mean (j) result. The thick solid line denotes the MLD in the historical simulation.

resent the sea surface net heat flux and ocean horizontal temperature advection effect on MLD change separately. In the north region, both $h_q^{'}$ and $h_t^{'}$ are benefit to deepen the MLD and the inter-model difference is not very large (Fig. 5a). In ensemble mean, $h_q^{'}$ (30.4 m/month) and $h_t^{'}$ (21.4 m/month) are comparable. In the south region, however, the sea surface net heat flux in most models deepen the MLD, but ocean horizontal temperature advection in all models shoal the MLD. In ensemble mean, $h_q^{'}$ (33.9 m/month) and $h_t^{'}$ (–29.0 m/month) are comparable in values but have a different sign, so the sum $\left(h_q^{'}+h_t^{'}\right)$ is just 4.9 m/month. This opposite effect causes the MLD in the south region shallower than that in the north region. The inter-model difference exists in both $h_q^{'}$ and $h_t^{'}$, but they have the same sign in most models. This quantitative result is consistent with the qualitative discussion mentioned above.

To analyze how the ocean horizontal temperature advection influences the MLD spatial pattern, the vertical-latitude sections of the temperature and temperature advection in models are shown in Fig. 6. The ocean horizontal temperature advection changes obviously from south to north. It is found that the cold advection exists in the north region and the strong warm advection exists in the south region in each model, as mentioned above. Further more, we find that the advection vertical maximum appears near the sea surface, and the advection decreases with the depth increasing. The vertical difference of the advection is benefit to weaken the ocean stratification in the north region, but increase it in the south region. This interesting phenomenon indicates that the Ekman advection may contribute more to the MLD than the geostrophic advection.

4.3 *The ocean current influence on the ocean advection*

Indicated from Fig. 4c and Fig. 6, the ocean current may be important for the formation of the nonuniform advection pattern, especially in the south region, so we focus on the ocean current effect in the south region as follows. Generally, the upper ocean current horizontal temperature advection *HTA* could be resolved into Ekman advection HTA_e and geostrophic advection HTA_g from Eq. (8). Both two advections could be resolved into east-west component U and north-south component V. As the east-west components are so small and could be ignored, HTA_e and HTA_g are both decided by the north-south components V in the south region (Fig. 7). While the northward warm V_e (Fig. 7b, dark gray bars, negative) is about twice of the southward cold V_g (Fig. 7b, light gray bars, positive) in all the models, so the total advection HTA is a warm advection (Fig. 7b, black bars, negative). In the ensemble mean, V_e is -1.75×10^{-7} K/s, V_g is 0.8×10^{-7} K/s, so V is about -0.85×10^{-7} K/s. This phenomenon indicates that the northward warm Ekman advection controls the upper ocean horizontal temperature advection and prevents the deepening of the MLD in the south region. Besides, it is inferred that the northward warm Ekman advection is dominated by the northwest Ekman horizontal velocity due to the northeast trade wind in this area.

As mentioned above, the northward warm Ekman advection controls the ocean horizontal temperature advection, and prevents the deepening of the MLD in the south region. While the southward cold advection deepens the MLD in the north region, as similar as the Ekman pumping and sea surface net heat flux. The nonuniform advection pattern controls the nonuniform MLD spatial pattern, and then induces the strong MLD front in this area. The northwest Ekman horizontal velocity due to the local northeast trade wind may play a critical role in the northward warm Ekman advection.

5 The influence of the MLD on the subduction

The MLD front plays an important role in the subduction process (Xie et al., 2000; Tsujino and Yasuda, 2004; Xu et al., 2016). As the effective subduction only occurs after the MLD reaches maximum, we calculate the subduction rate during February–March from Eq. (7). The lateral induction occurs at the current across the front of the MLD and the Ekman pumping velocity is determined by the sea surface wind curl (Xia et al., 2015). We could find that the subduction rate spatial patterns are similar in

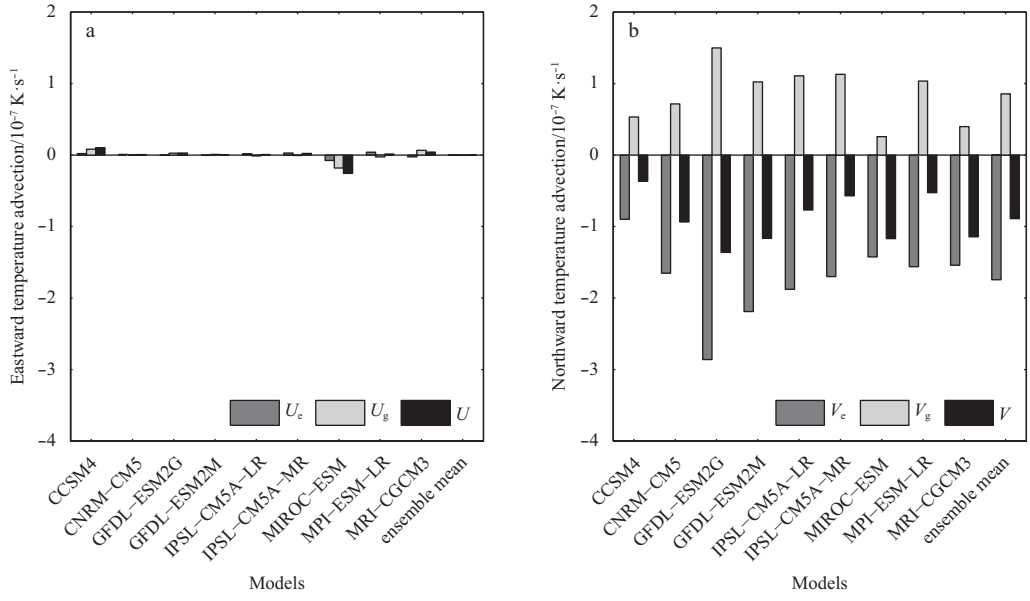

Fig. 7. The regional average Ekman advection HTA_e (dark gray bars), geostrophic advection HTA_g (light gray bars) and the total horizontal temperature advection HTA (black bars) in the south region upper 50 m during February–March in historical simulation of the nine models and ensemble mean result. a. East-west component U_e, U_g and U, and b. north-south component V_e, V_g and V.

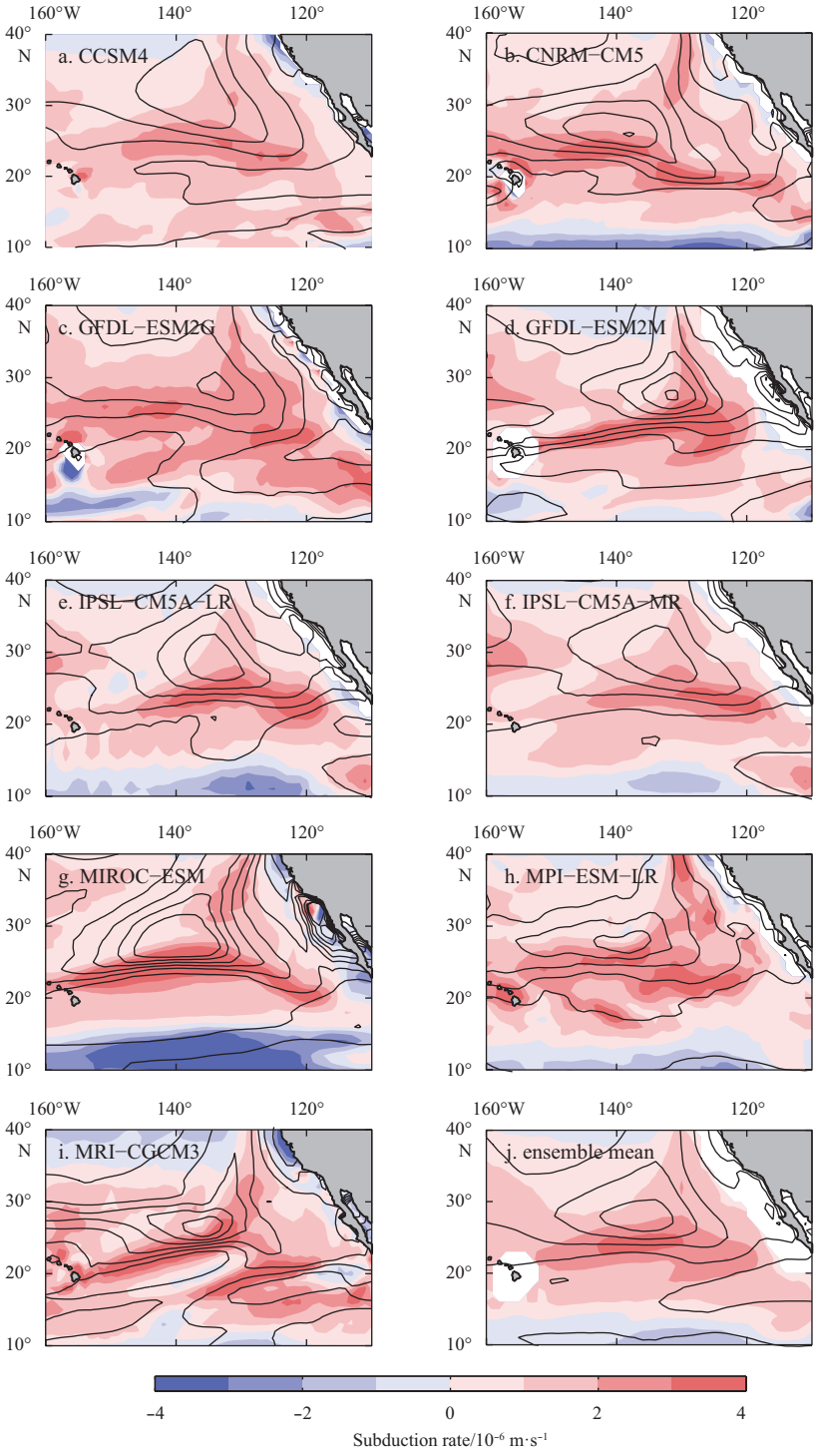

Fig. 8. The mean MLD (contours, interval: 20 m) and mean subduction rate (shading in m/s, downward is positive) during February–March in historical simulation of the nine models (a–i) and ensemble mean (j) result.

different models (Fig. 8). In the ensemble mean, the subduction maximum region forms a banded structure near east-west direction, with the maximum 4×10^6 m/s at (24°N, 140°W). Compare Fig. 8 with Fig. 9, the nonuniform subduction rate spatial parttern is almost dominated by the nonuniform lateral induction rate distribution. The latter is highly consistent with the position and intensity of the MLD front ∇h_{m} (Eq. (9)).

Figure 10 compares the relative contributions of the lateral induction and Ekman pumping rate to the subduction maximum from regional average (20°–28°N, 145°–120°W) in different models quantitatively. The Ekman pumping rate is close to the lateral induction rate in most models, even larger in some models such as CNRM-CM5 and GFDL-ESM2G. In the ensemble mean, the contributions of Ekman pumping (1.6×10^6 m/s) and lateral induction rate (1.3×10^6 m/s) to the subduction rate (2.9×10^6 m/s) seem equal in the chosen region. Nevertheless, inter-model difference of the Ekman pumping rate is much smaller than that of the lateral induction rate, which means that the inter-model dif-

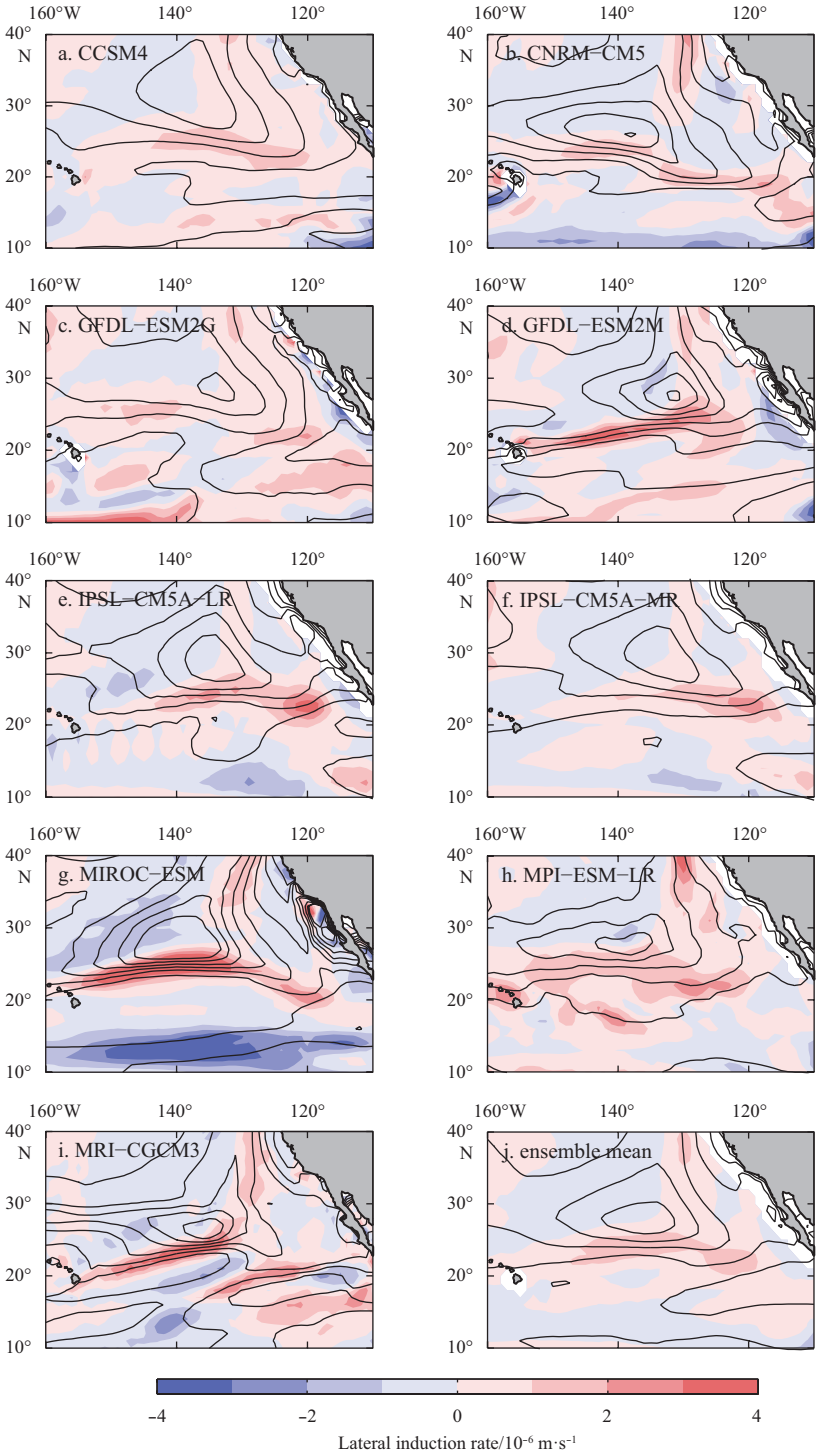

Fig. 9. The mean MLD (contours, interval: 20 m) and mean lateral induction rate (shading in m/s, downward is positive) during February–March in historical simulation of the nine models (a–i) and ensemble mean (j) result.

ference of subduction is mainly caused by the inter-model difference of lateral induction.

6 Conclusions

In this paper, we have examined the climatology characteristics of the MLD in the subtropical Northeast Pacific in present-day climate, compared the MLD based on nine of the CMIP5 models results and two observation data. It exists a local maximum MLD region centered at (28°N, 135°W) in late winter, where the ensemble mean maximum value can exceed 140 m in the modeling results. The spatial pattern of the MLD is nonuniform, causing a strong MLD front on the south of the maximum region, which is similar to that in the observation. In other words, the MLD has a inter-regional difference, which is much deeper (>140 m) in the north region and relatively shallower (<60 m) in the south region. There are obviously seasonal variations in the MLD spatial pattern, and the MLD reaches its seasonal maximum in February–March in modeling results.

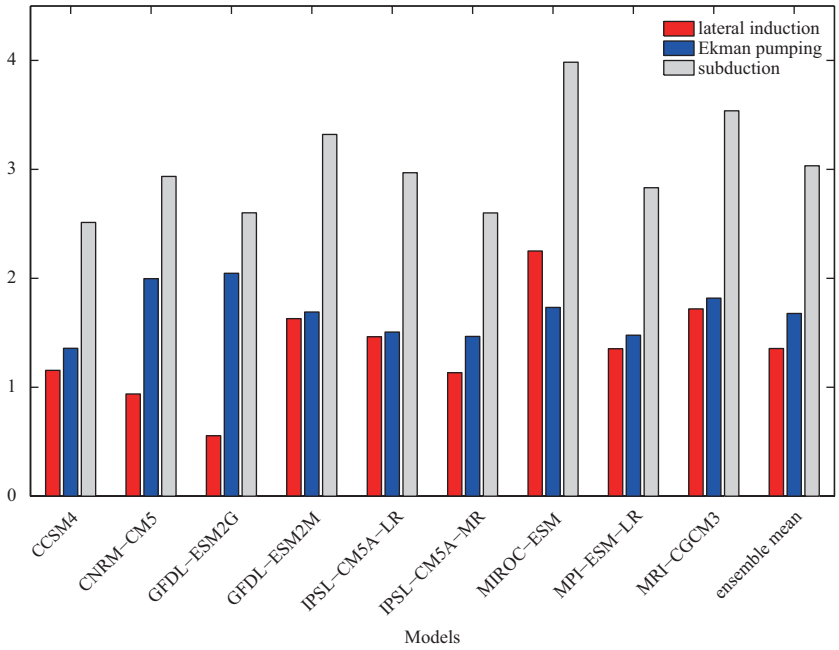

Fig. 10. The regional average (20°–28°N, 145°–120°W) lateral induction rate (red bars, unit: 10^{-6} m/s), Ekman pumping rate (blue bars, unit: 10^{-6} m/s) and subduction rate (gray bars, unit: 10^{-6} m/s) during February–March in historical simulation of the nine models and ensemble mean result.

The strong MLD front caused by nonuniform MLD controls the lateral induction rate pattern, then decides the nonuniform distribution of the subduction rate. The relatively uniform Ekman pumping has little effect on the nonuniform subduction spatial parttern, though it is nearly equal to the lateral induction in values. As the subduction process impacts on the formation of ESTMW significantly, the nonuniform MLD spatial pattern occupies an important position in this physical process.

This study focuses on the mechanisms of the nonuniform MLD spatial pattern. It is demonstrated that the northward warm Ekman advection controls the upper ocean horizontal temperature advection, especially in the south region. From the south region average in the ensemble mean, the northward warm Ekman advection V_e is -1.75×10^{-7} K/s, while the southward cold geostrophic advection V_g is 0.8×10^{-7} K/s, so the sum advection *HTA* is carried northward (-0.85×10^{-7} K/s). The ocean advection prevents the deepening of the MLD in the south region. The contribution of the ocean advection to the MLD is about 29.0 m/month in the ensemble mean, leading to offset the heat flux contribution (33.9 m/month). While in the north region, the southward cold advection deepens the MLD (21.4 m/month) as similar as the sea surface net flux (30.4 m/month). As the inter-regional differences of the Ekman pumping and sea surface net flux in both regions are relatively small, the nonuniform MLD spatial pattern is mainly controlled by the nonuniform ocean horizontal temperature advection, and then induces the strong MLD front in this area. Finally, we inferred that the northwest Ekman horizontal velocity is caused by the local northeast trade wind.

Acknowledgements

The authors appreciate World Climate Research Programme's Working Group on Coupled Modeling, which is responsible for CMIP5, and thank the climate modeling groups (listed in Table 1) for producing and making available their model output.

References

Carton J A, Giese B S. 2008. A reanalysis of ocean climate using Simple Ocean Data Assimilation (SODA). Monthly Weather Review, 136(8): 2999–3017

Dawe J T, Thompson L A. 2007. PDO-related heat and temperature budget changes in a model of the North Pacific. Journal of Climate, 20(10): 2092–2108

de Boyer Montégut C, Madec G, Fischer A S, et al. 2004. Mixed layer depth over the global ocean: an examination of profile data and a profile-based climatology. Journal of Geophysical Research, 109(C12): C12003

Deser C, Blackmon M L. 1995. On the relationship between tropical and North Pacific sea surface temperature variations. Journal of Climate, 8(6): 1677–1680

Dong Shenfu, Sprintall J, Gille S T, et al. 2008. Southern Ocean mixed-layer depth from Argo float profiles. Journal of Geophysical Research, 113(C6): C06013

Dunne J P, John J C, Adcroft A J, et al. 2012. GFDL's ESM2 global coupled climate-carbon earth system models. Part I: physical formulation and baseline simulation characteristics. Journal of Climate, 25(19): 6646–6665

Hu Haibo, Liu Qinyu, Zhang Yuan, et al. 2011. Variability of subduction rates of the subtropical North Pacific mode waters. Chinese Journal of Oceanology and Limnology, 29(5): 1131–1141

Kara A B, Rochford P A, Hurlburt H E. 2003. Mixed layer depth variability over the global ocean. Journal of Geophysical Research, 108(C3): 3079

Kraus E B. 1972. Atmospheric–Ocean Interaction. London: Oxford University Press, 255

Levitus S. 1982. Climatological atlas of the world ocean. Eos, Transactions American Geophysical Union, 64(49): 962–963

Levitus S, Boyer T P. 1994. World Ocean Atlas 1994. Volume 4, Temperature. Washington, DC: National Environmental Satellite, Data, and Information Service

Liu Chengyan, Wang Zhaomin. 2014. On the response of the global subduction rate to globalwarming in coupled climate models. Advances in Atmospheric Sciences, 31(1): 211–218

Liu Chengyan, Wang Zhaomin, Li Bingrui, et al. 2017. On the response of subduction in the South Pacific to an intensification

of westerlies and heat flux in an eddy permitting ocean model. Advances in Atmospheric Sciences, 34(4): 521–531

Liu Chengyan, Wu Lixin. 2012. An intensification trend of South Pacific mode water subduction rates over the 20th century. Journal of Geophysical Research, 117(C7): C07009

Luo Yiyong, Liu Qinyu, Rothstein L M. 2009. Simulated response of North Pacific Mode Waters to global warming. Geophysical Research Letters, 36(23): L23609

Marshall J C, Nurser A J G, Williams R G. 1993. Inferring the subduction rate and period over the North Atlantic. Journal of Physical Oceanography, 23(7): 1315–1329

Monterey G I, Levitus S. 1997. Climatological Cycle of Mixed Layer Depth in the World Ocean. Washington DC: U.S. Government Printing Office, NOAA NESDIS, 5

Pan Aijun, Wan Xiaofang, Liu Qinyu. 2011. Diagnostics of mixed-layer thermodynamics in the formation regime of the North Pacific subtropical mode water. Journal of Tropical Oceanography (in Chinese), 30(5): 8–18

Pond S, Pickard G L. 1983. Introductory Dynamical Oceanography. 2nd ed. New York: Pergamon, 379

Qiu Bo. 2002. The Kuroshio Extension system: its large-scale variability and role in the midlatitude ocean-atmosphere interaction. Journal of Oceanography, 58(1): 57–75

Qiu Bo, Chen Shuiming. 2006. Decadal variability in the formation of the North Pacific Subtropical Mode Water: oceanic versus atmospheric control. Journal of Physical Oceanography, 36(7): 1365–1380

Qiu Bo, Kelly K A. 1993. Upper-ocean heat balance in the Kuroshio Extension region. Journal of Physical Oceanography, 23(9): 2027–2041

Qu Tangdong, Chen Ju. 2009. A North Pacific decadal variability in subduction rate. Geophysical Research Letters, 36(22): L22602

Stommel H. 1979. Determination of water mass properties of water pumped down from the Ekman layer to the geostrophic flow below. Proceedings of the National Academy of Sciences of the United States of America, 76(7): 3051–3055

Suga T, Motoki K, Aoki Y, et al. 2004. The North Pacific climatology of winter mixed layer and Mode Waters. Journal of Physical Oceanography, 34(1): 3–22

Toyoda T, Awaji T, Ishikawa Y, et al. 2004. Preconditioning of winter mixed layer in the formation of North Pacific Eastern Subtropical Mode Water. Geophysical Research Letters, 31: L17206

Taylor K E, Stouffer R J, Meehl G A. 2012. An overview of CMIP5 and the experiment design. Bulletin of the American Meteorological Society, 93(4): 485–498

Tsujino H, Yasuda T. 2004. Formation and circulation of mode waters of the North Pacific in a high-resolution GCM. Journal of Physical Oceanography, 34(2): 399–415

Williams R G. 1991. The role of the mixed layer in setting the potential vorticity of the main thermocline. Journal of Physical Oceanography, 21(12): 1803–1814

Woods J D. 1985. The physics of pycnocline ventilation. In: Nihoul J C J, ed. Coupled Ocean-Atmosphere Models. London: Elsevier, 543–590

Xia Ruibin, Liu Qinyu, Xu Lixiao, et al. 2015. North Pacific eastern subtropical mode water simulation and future projection. Acta Oceanologica Sinica, 34(3): 25–30

Xie Shangping, Deser C, Vecchi G A, et al. 2010. Global warming pattern formation: sea surface temperature and rainfall. Journal of Climate, 23(4): 966–986

Xie Shangping, Kunitani T, Kubokawa A, et al. 2000. Interdecadal thermocline variability in the North Pacific for 1958-97: a GCM simulation. Journal of Physical Oceanography, 30(11): 2798–2813

Xie Shangping, Xu Lixiao, Liu Qinyu, et al. 2011. Dynamical role of mode water ventilation in decadal variability in the central subtropical gyre of the North Pacific. Journal of Climate, 24(4): 1212–1225

Xu Lixiao, Li Peilaing, Xie Shangping, et al. 2016. Observing mesoscale eddy effects on mode-water subduction and transport in the North Pacific. Nature Communications, 7: 10505

Xu Lixiao, Xie Shangping, Liu Qinyu, et al. 2012. Response of the North Pacific subtropical countercurrent and its variability to global warming. Journal of Oceanography, 68(1): 127–137